Retrieval of precipitable water using ADEOS-II / GLI near infrared data

Makoto Kuji*[a], Nobuyuki Kikuchi[b], and Akihiro Uchiyama[c]

[a] *Dept. of Information and Computer Sciences, Nara Women's Univ., Japan*
[b] *Earth Observation Research and application Center, Japan Aerospace Exploration Agency, Japan*
[c] *Meteorological Research Institute, Japan Meteorological Agency, Japan*

ABSTRACT

Retrieval of vertically integrated water vapor amount (precipitable water) is proposed using near infrared channels of Global Imager onboard Advanced Earth Observing Satellite-II (GLI / ADEOS-II). The principle of retrieval algorithm is based upon that adopted with Moderate Resolution Imaging Spectroradiometer (MODIS) onboard Earth Observing System (EOS) satellite series. Simulations were carried out with GLI Signal Simulator (GSS) to calculate the radiance ratio between water vapor absorbing bands and non-absorbing bands. As a result, it is found that for the case of high spectral reflectance background (a bright target) such as the land surface, the calibration curves are sensitive to the precipitable water variation. It turns out that aerosol loading has little influence on the retrieval over a bright target for the aerosol optical thickness less than about 1.0 at 500 nm wavelength. A preliminary analysis of GLI data was also carried out and the retrieved result is compared to radiosonde observations. In spite of a lag of several hours between the ADEOS-II / GLI and the radiosonde observations, the retrieved precipitable water values were coincident to those of in situ observations within 2.0 mm at a few radiosonde sites. Currently, we are trying to make fully simultaneous comparisons of the retrieved precipitable water values to those derived from continuous observations with skyradiometers or microwave radiometers. As a result, we will validate the accuracy of the retrieval algorithm for the purpose of its global application. It is also anticipated that simultaneous retrieval of the water vapor amount using GLI data along with other channels will lead to improved accuracy of the determination of surface geophysical properties, such as vegetation, ocean color, and snow and ice, through the better atmospheric correction.

Key Words: water vapor, near infrared, ADEOS-II / GLI.

1. INTRODUCTION

Water vapor is one of typical gas species governing the greenhouse effect. Investigation of water vapor distribution is a clue to understand the radiation budget of earth atmosphere system as well as the global energy and hydrological circulation. Although water vapor is mostly distributed in the lower atmosphere (planetary boundary layer from surface to a few kilometers), the water vapor amount often increases in the middle and upper troposphere accompanying horizontal advection of humid air mass. Thus, precipitable water, (i.e. the vertically integrated water vapor amount) is considered to be the most representative quantity of water vapor amount in the atmosphere.

Until now, TIROS-N Operational Vertical Sounder (TOVS) data have been often used to estimate water vapor amount at lower, middle, and upper regions of the troposphere [1]. Although TOVS is a splendid vertical sounder with a number of channels sensitive to water vapor absorption, their footprints are about several tens kilometers, rather larger than those of environmental sensors onboard earth-observing satellites. Better spatial resolutions of several hundred meters to several kilometers are available with MODIS / EOS sensors, wavelengths and bandwidths of which are very similar to those of TOVS. Combining the near infrared data of water vapor absorbing and non-absorbing channels with the thermal infrared data, precipitable water is derived from the MODIS mission with a relatively high spatial resolution along with information of clouds and aerosols [2].

In contrast to TOVS and MODIS, GLI onboard ADEOS-II is designed to obtain data of both the surface properties (vegetation, ocean color, and snow and ice, etc.) and atmospheric properties (cloud, aerosol, and radiation budget, etc.). In

general, atmospheric correction is indispensable when surface geophysical properties are retrieved from satellite remote sensing data. Correction of atmospheric ozone, aerosol, and in particular, water vapor is important for precise retrieval of vegetation conditions and ocean color. In the GLI mission, it is currently planned that the water vapor information is incorporated from the quasi-real-time objective analysis data. Nevertheless, it is desirable to use the water vapor information concurrently obtained with the same spatial resolution as other channels. In this context, we study feasibility of using near infrared channels of GLI in the retrieval of precipitable water and make a preliminary analysis of the GLI data and its validation. The principle of the retrieval algorithm is described in Sec. 2 together with assumptions made in the present simulation. In Sec. 3, retrieved precipitable water is analyzed and validated with radiosonde observation. Section 4 presents the summary and related future works.

2. RETRIEVAL ALGORITHM AND SIMULATION

2.1 Principle

The retrieval algorithm is based upon the radiance ratio method, which utilizes the radiance ratio between water vapor absorbing and non-absorbing bands to retrieve the precipitable water. A similar method was already adopted with MODIS / EOS series [3, 4]. In the MODIS case, 940 nm and 865 nm bands were utilized as the water vapor absorbing band and non-absorbing band [3], respectively, and the retrieved results on a global scale were already reported [4].

Principle of the retrieval algorithm is explained concisely here. Figure 1 illustrates transmittance curves of water vapor in the near infrared region, calculated using the LOWTRAN 7 code [5]. As seen from Fig. 1, water vapor absorbing bands (spectral regions with smaller transmittance) are located at around 810 nm, 940 nm, 1135 nm, and 1380 nm, whereas non-absorbing bands (regions with larger transmittance; i.e., atmospheric window region) are found at 865 nm, 1050 nm, and 1240 nm. The six atmospheric models and their values for precipitable water are summarized in Table 1. The retrieval algorithm utilizes these characteristics as follows: in the water vapor absorbing bands, transmittance (i.e., radiance to be observed) varies with the water vapor amount (precipitable water) assumed in each atmospheric model, while in the non-absorbing bands, changes are much smaller.

Table 1 Atmospheric models and their precipitable water.

Model Atmosphere	Precipitable Water (mm)
Tropical	40.0
Midlatitude Summer	28.5
Subarctic Summer	20.4
US Standard 1976	13.9
Midlatitude Winter	8.38
Subarctic Winter	4.10

For the GLI application, here we propose a retrieval method in which calibration curves are determined between the radiance ratio of water vapor absorbing band (e.g., Ch. 25; 1135 nm) to non-absorbing band (e.g., Ch. 26; 1240 nm) and water vapor amount (precipitable water) in a form of nonlinear regression. The GLI channel specifications related to this feasibility study are summarized in Table 2 [6].

Table 2 Related Channel Specifications of GLI.

Channel Number	Central Wavelength (nm)	Band Width (nm)	IFOV [a] (km)	Maximum Radiance [b]	SNR [d]	Comment
19	865	10	1	228 [c]	97.5 [c]	Window Region
24	1050	20	1	203	300	Window Region
25	1135	70	1	200	350	Water Vapor
26	1240	20	1	138	70	Window Region
27	1380	40	1	94	120	Water Vapor

[a] Instantaneous Field of View.

[b] In units of W m^{-2} sr^{-1} m^{-1}.

[c] These values were attenuated by 25 % from the original ones [3].

[d] Signal to Noise Ratio.

Based upon the principle of the retrieval algorithm, the channel which is most sensitive to variation of water vapor amount is chosen as a water vapor absorption channel and, on the other hand, the one which is least sensitive to it as a non-absorbing channel. As seen from Fig. 1, there are two water vapor absorbing bands in the near infrared region, Ch. 25 (1135 nm) and Ch. 27 (1380 nm). Between two channels, Fig. 1 also indicates that Ch. 25 (with a band width of 70 nm) is more sensitive to the variation of water vapor amount than Ch. 27 (40 nm). As a result, Ch. 25 (1135 nm) is selected as a water vapor absorbing channel. For non-absorbing bands, there are three channels, Ch. 19 (865 nm), Ch. 24 (1050 nm), and Ch. 26 (1240 nm). From Fig. 1, it is expected that Ch. 26 (with a band width of 20 nm) is more sensitive to the variation than other two channels: Ch. 19 (10 nm) and Ch. 24 (20 nm). The magnitude of radiance of Ch. 19 (865 nm), however, is much larger than those of Ch. 25 (1135 nm), which leads to the smaller dynamic range of the radiance ratio (defined later). As a result, Ch. 26 (1240 nm) is selected as non-absorbing channels.

Simulations were carried out with the GLI Signal Simulator (GSS) [7] so as to calculate radiances to be observed at the GLI / ADEOS-II. The code enables us to calculate the radiance to be observed with GLI, assuming several atmospheric models including aerosol loading as well as water vapor. In the previous feasibility study, two cases of a bright target (land) and a dark target (ocean) are considered as ground surfaces with the GSS simulations [9] and we present the bright target analyses in this study.

The land model is assumed as a Lambertian surface whose spectral reflectance is 50 %,

chosen as a representative case of a bright target. This assumption is based upon the grass model in the ASTER spectral library [8], which shows surface reflectance of 50.7 %, and 48.8 % for 1135 nm, and 1240 nm spectral region, respectively. For simplicity, the effect of bidirectional reflectance distribution function is not considered in this study. Simulations were carried out under clear sky conditions. Moreover, the effect of aerosol loading in the model atmosphere was also examined. For the aerosol model, a rural one incorporated in the GSS was utilized over land [7].

The upward radiances at the top of the atmosphere were simulated for the following case: over a bright target (i.e., land). Two bands, that is, one water vapor absorbing channel (1135 nm) and one non-absorbing channels (1240 nm), was used to carry out simulations, that is, the combination of 1135 nm and 1240 nm was examined to calculate the radiance ratio. In addition, the following case is assumed for scan geometry: solar zenith angle 60°, satellite zenith angle 60°, and relative azimuthal angle 90°.

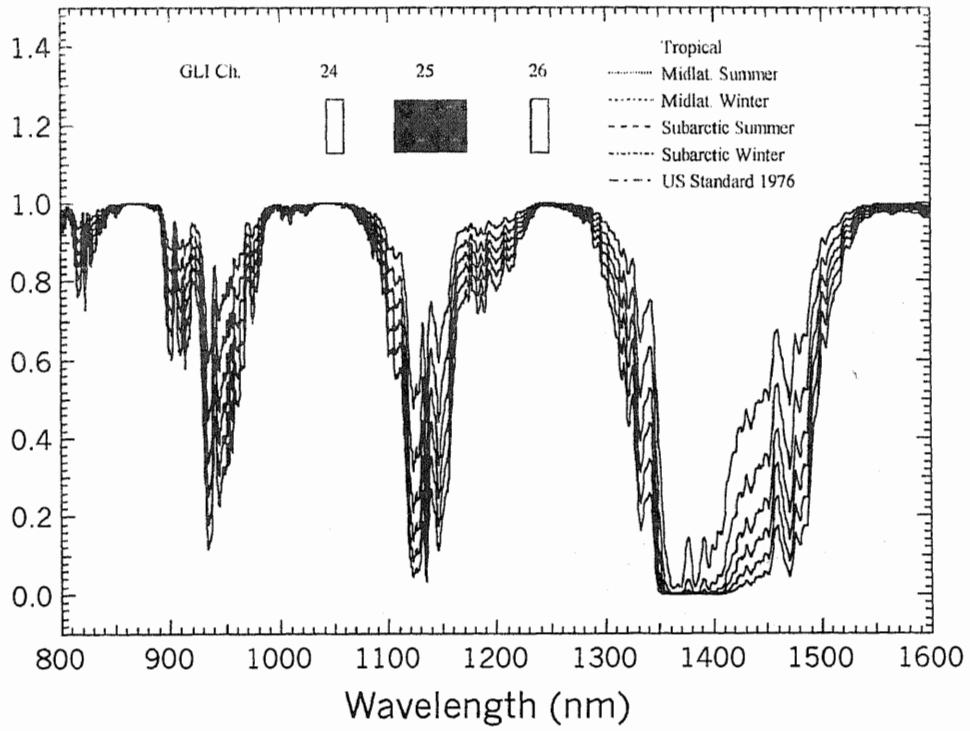

Fig. 1. Atmospheric transmittance related to water vapor in the near infrared spectral region between 800 nm to 1600 nm. Curves are calculated with the LOWTRAN 7 code for vertical one way path, as products between water vapor absorption lines and continuum absorption. The six transmittance lines correspond to the six model atmospheres listed in Table 1. Closed and open rectangles are the spectral ranges of the GLI for water vapor absorbing and window channels, respectively.

2.2 Retrieval algorithm

In this study, the radiance ratio (T_w) is defined as

$$T_w(ch1,ch2) \equiv \frac{R_{ch1}}{R_{ch2}}, \qquad (1)$$

where $ch1$ indicates a water vapor absorbing channel (i.e., 1135 nm), at which radiation undergoes strong absorption due to water vapor, $ch2$ is a non-absorbing channel (i.e., 1240 nm), and R is the radiance simulated with the GSS at the top of the atmosphere for the specified channel. This definition is essentially equivalent to that of Kaufman and Gao [3], except for a factor originating from the ratio of the

extraterrestrial solar incident irradiances between the specified channels.

Based upon the above definition, a relationship (a calibration curve) is proposed between the radiance ratio (T_w) and the precipitable water (W):

$$T_w(ch1,ch2) = a + b\exp\left(-c\sqrt{W}\right), \qquad (2)$$

where a, b and c are calibration coefficients. If the coefficient a is set to zero, this relationship is equivalent to that of Kaufman and Gao [3], since the effect of the solar terrestrial incident irradiance was implicitly included in the coefficient b. Here the coefficient a is added explicitly to consider a bias that arises from the molecular scattering and aerosol loading effects [9].

In order to study the effect of scan geometry on the calibration curve, the precipitable water (W) is converted to the water vapor path (W^*). The relationship between these two parameters is given as

$$W^* = W\left(\frac{1}{\cos\theta} + \frac{1}{\cos\theta_0}\right), \qquad (3)$$

where θ and θ_0 are the satellite and solar zenith angles, respectively. Using W^* instead of W, Eq. (2) is modified as

$$T_w(ch1,ch2) = a^* + b^*\exp\left(-c^*\sqrt{W^*}\right). \qquad (4)$$

In the following analysis, radiance ratios (T_w) are calculated with Eq. (1) from the radiances simulated with the GSS, and least-squares fitting procedures are carried out with Eq. (4)

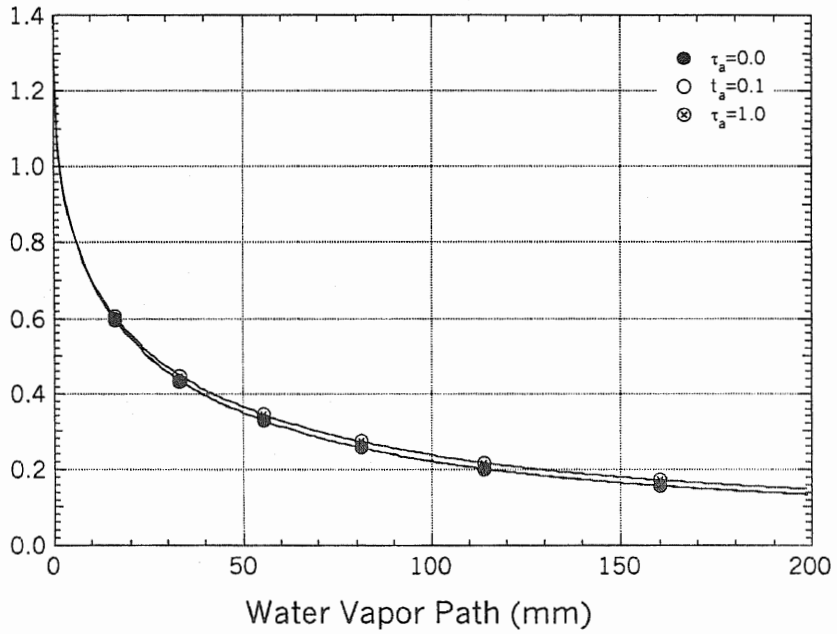

Fig. 2. Calibration curves between the radiance ratio and scaled water vapor path under rural aerosol loading (τ_a=0.0, 0.1, and 1.0) conditions over a bright target (land). All circles denote the radiance ratio between the 1135 nm and 1240 nm channels and are fitted with the calibration curves (Eq. (4)). All the cases are for a scan geometry of solar zenith angle 60°, satellite zenith angle 60°, and relative azimuthal angle 90°.

2.3 Simulations over a bright target with aerosol loading

Figure 2 shows relationships between radiance ratio and water vapor path simulated with the six atmospheric models in Table 1. This is the case with the solar zenith angle 60°, satellite zenith angle 60°, and relative azimuthal angle 90°. In order to minimize the effect of scan geometry, scaled water vapor path in Eq. (3) is used instead of the precipitable water. Here we investigated the effect of aerosol loading on

the retrieval sensitivity under clear atmospheric conditions, too. Simulations with the GSS were carried out with the six model atmospheres over a bright target while changing the aerosol optical thickness at 500 nm (τ_a) as 0.0, 0.1, and 1.0 over a bright target with rural aerosol loading. Apparently, all the three cases are fitted well with the calibration curves in Eq. (4) and the curves are almost identical to each other. This indicates that the use of water vapor path enables us to retrieve the precipitable water from the observed radiance ratio over bright targets (e.g., land surfaces), even under moderate aerosol loading. In this simulation, the land surface reflectances were assumed to be 50 % for all the two channels. Consequently, the reflectance ratios of land surface are unity. But, even using the land surface reflectances in the ASTER spectral library [8], they are actually 1.04 for R_{1135}/R_{1240}. It turns out that this assumption is not influential to the results very much in the simulations.

3. APPLICATION TO GLI DATA AND ITS VALIDATION

The algorithm was applied to the GLI data set as a preliminary analysis. The images of the relevant GLI data are illustrated in Fig. 3. There extends huge cloud system over the western part of the North American continent around California. Cloudy pixels are not retrieved, since the algorithm is applicable only over land and snow/ice surfaces, currently. Comparing these two panels, an apparent difference exists near the cloud edge over the California peninsula: there are darker pixels in the water vapor absorbing channel (Fig. 3a) compared to the non-absorbing one (Fig. 3b).

The retrieval procedure is as follows: At first, cloud screening based upon GLI processing system is carried out. Once the available pixels are determined, the radiance ratio (T_w) is calculated with the two-channel data as describe in Eq. (1). And then, the scaled water vapor path (W^*) was estimated with Eq. (4). Using the solar and satellite zenith angles of the pixels concerned, precipitable water (W) is estimated with Eq. (3) from the water vapor path. A map of precipitable water retrieved above procedure is illustrated in Fig. 4.

(a) (b)

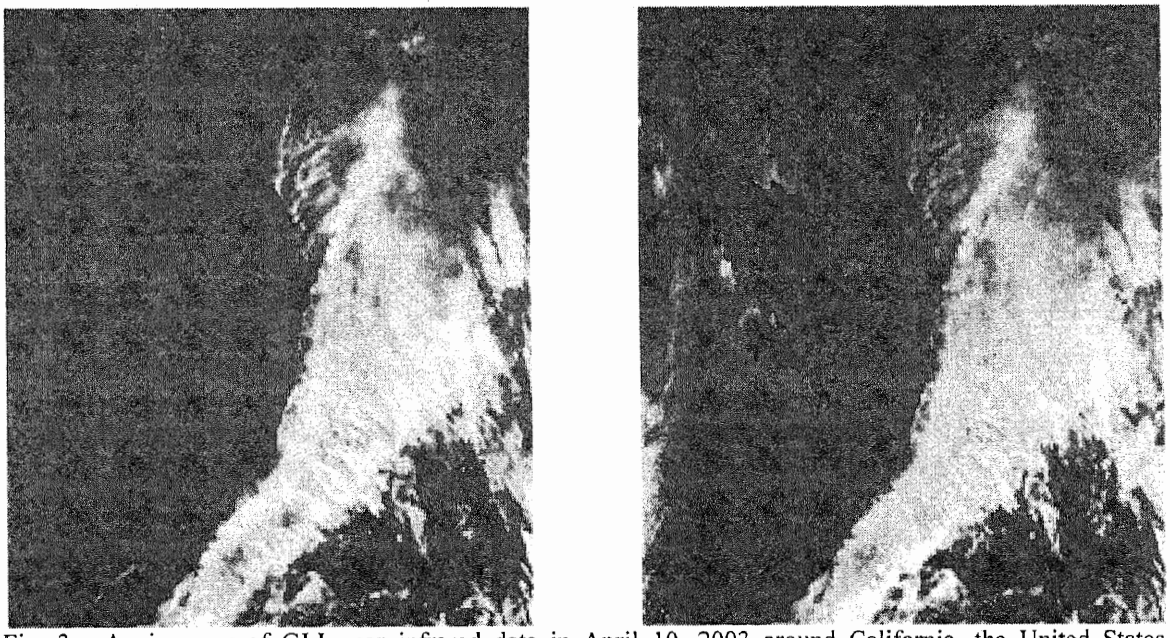

Fig. 3. An imagery of GLI near infrared data in April 10, 2003 around California, the United States of America: (a) ch25 (1135nm), (b) ch26 (1240nm). The channels 25 and 26 are a water vapor absorbing and a no-absorbing channel, respectively. There extended cloud system from the western part of a North American continent to the eastern Pacific Ocean.

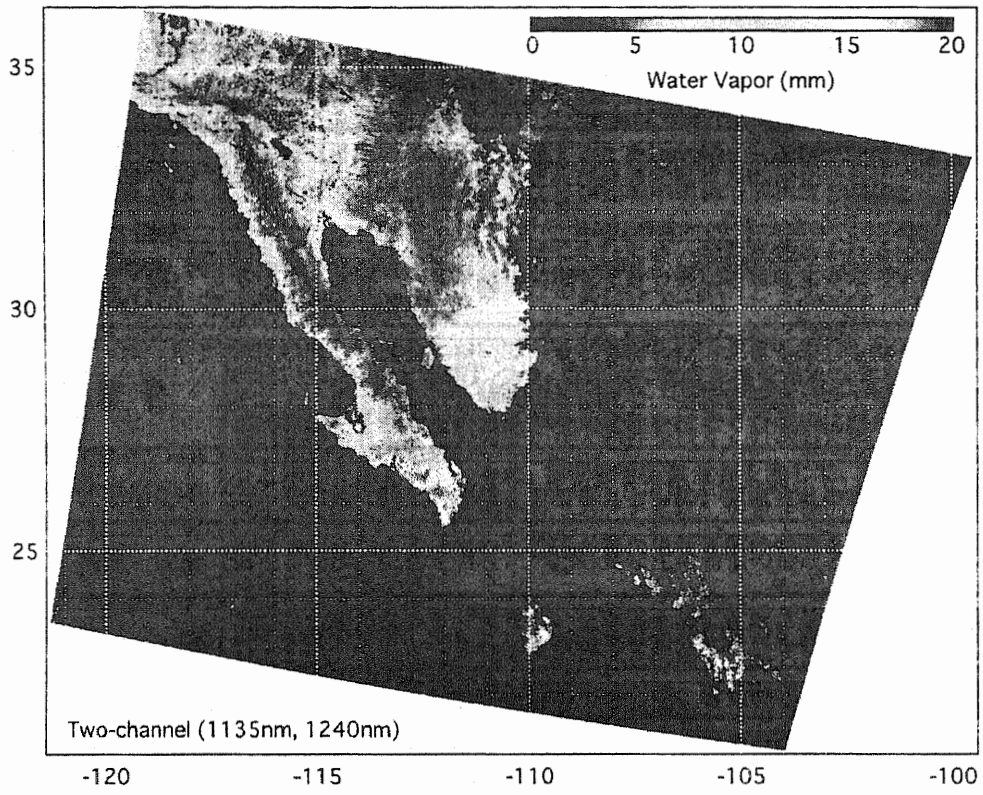

Fig. 4. A retrieved precipitable water distribution in unit of mm in April 10, 2003. The radiance ratio between two channels (1135 nm and 1240 nm) was utilized in the retrieval. The retrieval was performed only over land and snow/ice regions, that is, it was not carried out over cloud and water (ocean). The distribution is mapped on the iso-latitude and iso-longitude coordinate. The numbers around the left and bottom frames denote latitude (°N) and loingitude (°E), respectively. Here, a minus sign corresponds to a western longitude.

Table 3 Comparison of precipitable water. Observation time is 1200 UTC for every radiosonde event.

Site # *	Location		Precipitable water (mm)	
	Latitude (°W)	Longitude (°W)	GLI	Radiosonde
72293	32.83	117.12	7.3	6.9
72274	32.12	110.93	1.5	4.9
76256	27.95	110.77	11.6	10.3

* WMO site number (five digits).

As is expected with comparison of these two channels, much precipitable water was observed at the southern part of the California peninsula next to the cloudy pixels. At the northern part of the peninsula, on the other hand, there existed much smaller water vapor amount corresponding to the mountain features.
The retrieved precipitable water was compared to the radiosonde observations. Table 3 summarizes the validation. The radiosonde observation suggests that the differences between retrieved and in situ observation is about 1-2 mm for a few radiosonde sites. There was a case that had a severe discrepancy (up to factor 3) between satellite and in situ observations, however. The comparison showed the further validation study was necessary since radiosonde observation (00 and 12 UTC) is not fully coincident to the ADEOS-II / GLI operation (around 10:30 AM at local time). We have a plan to compare the retrieved values to skyradiometer and microwave radiometer observations.

4. SUMMARY AND CONCLUDING REMARKS

We have proposed the retrieval of water vapor amount (precipitable water) using GLI near infrared channels. The retrieval approach proposed in this study enables us to retrieve water vapor amount using GLI onboard ADEOS-II. The results of simulations indicate that the radiance ratio between 1135 nm and 1240 nm channels is well sensitive to the precipitable water over a bright target (higher reflectance at ground level) with Lambertian reflectivity. Over a bright target with spectral reflectance of 50 %, aerosol loading with optical thickness (at 500 nm) of less than 1.0 is not influential to the calibration curves of the retrieval.
The retrieval algorithm was applied to the GLI data around western part of the United States of America. In this preliminary analysis, the retrieval procedure worked well in the GLI data analysis system in JAXA / EORC. The retrieved results were compared to the radiosonde observation sites and the retrieved precipitable water is coincident within 2 mm at a few sites. We have a plan to compare the retrieved results with the continuous observations such as skyradiometer and microwave radiometer sites for the purpose of its global application.

ACKNOWLEDGMENTS

The authors thank GLI Algorithm Integration Team (GAIT) / EORC / JAXA for simulations with GSS and the GLI data handling. This study was supported by Japan Aerospace Exploration Agency (A2-RA-G-0030).

REFERENCES

1. B. J. Soden and F. P. Bretherton: Interpretation of TOVS water vapor radiances in terms of layer-average relative humidities: Method and climatology for the upper, middle, and lower troposphere. *J. Geophys. Res.*, **101**, pp. 9333-9343, 1996.
2. M. D. King, Y. J. Kaufman, W. P. Menzel, and D. Tanre: Remote sensing of cloud, aerosol, and water vapor properties from the moderate resolution imaging spectrometer (MODIS). *IEEE Trans. Geoscience and Remote Sensing*, **30**, pp. 2-27, 1992.
3. Y. J. Kaufman and B.-C. Gao: Remote sensing of water vapor in the near IR from EOS/MODIS. *IEEE Trans. Geoscience and Remote Sensing*, **30**, pp. 871-884, 1992.
4. B.-C. Gao and Y. J. Kaufman: Remote sensing of water vapor and thin cirrus clouds using MODIS near-IR channels. *Proc. of SPIE*, **4150**, pp. 217-224, 2000.
5. F. X. Kneizys, E. P. Shettle, L. W. Abreu, J. H. Chetwynd, G. P. Anderson, W. O. Gallery, J. E. A. Selby, and S. A. Clough: Users guide to LOWTRAN 7. AFGL-TR-88-0177, 146 pp, 1988.
6. T. Y. Nakajima, T. Nakajima, M. Nakajima, H. Fukushima, M. Kuji, A. Uchiyama, and M. Kishino: The

optimization of the Advanced Earth Observing Satellite II Global Imager channels by use of radiative transfer calculations. *Appl. Opt.*, **37**, pp. 3149-3163, 1998.

7. T. Nakajima, T. Y. Nakajima, M. Nakajima, and GLI Algorithm Integration Team (GAIT): Development of ADEOS-II/GLI operational algorithm for earth observation. *Proc. of SPIE*, **3870**, pp. 314-322, 1999.
8. http://speclib.jpl.nasa.gov/archive/jhu/becknic/vegetation/txt/grass.txt
9. M. Kuji and A. Uchiyama: Retrieval of precipitable water using near infrared channels of Global Imager / Advanced Earth Observing Satellite-II (GLI / ADEOS-II). *J. Remote Sens. Soc. Japan*, **22**, pp. 149-162, 2002.